

This is the peer reviewed version of the following article:

Evidence of catalase mimetic activity in $\text{Ce}^{3+}/\text{Ce}^{4+}$ doped bioactive glasses / Nicolini, Valentina; Gambuzzi, Elisa; Malavasi, Gianluca; Menabue, Ledi; Menziani, Maria Cristina; Lusvardi, Gigliola; Pedone, Alfonso; Benedetti, Francesco; Luches, Paola; D'Addato, Sergio; Valeri, Sergio. - In: JOURNAL OF PHYSICAL CHEMISTRY. B, CONDENSED MATTER, MATERIALS, SURFACES, INTERFACES & BIOPHYSICAL. - ISSN 1520-6106. - ELETTRONICO. - 119:10(2015), pp. 4009-4019. [10.1021/jp511737b]

Terms of use:

The terms and conditions for the reuse of this version of the manuscript are specified in the publishing policy. For all terms of use and more information see the publisher's website.

18/12/2025 18:59



Article

Evidence of Catalase Mimetic Activity in Ce/Ce Doped Bioactive Glasses

Valentina Nicolini, Elisa Gambuzzi, Gianluca Malavasi, Ledi Menabue, Maria Cristina Menziani, Gigliola Lusvardi, Alfonso Pedone, Francesco Benedetti, Paola Luches, Sergio D'Addato, and Sergio Valeri

J. Phys. Chem. B, **Just Accepted Manuscript** • DOI: 10.1021/jp511737b • Publication Date (Web): 24 Feb 2015

Downloaded from <http://pubs.acs.org> on February 26, 2015

Just Accepted

"Just Accepted" manuscripts have been peer-reviewed and accepted for publication. They are posted online prior to technical editing, formatting for publication and author proofing. The American Chemical Society provides "Just Accepted" as a free service to the research community to expedite the dissemination of scientific material as soon as possible after acceptance. "Just Accepted" manuscripts appear in full in PDF format accompanied by an HTML abstract. "Just Accepted" manuscripts have been fully peer reviewed, but should not be considered the official version of record. They are accessible to all readers and citable by the Digital Object Identifier (DOI®). "Just Accepted" is an optional service offered to authors. Therefore, the "Just Accepted" Web site may not include all articles that will be published in the journal. After a manuscript is technically edited and formatted, it will be removed from the "Just Accepted" Web site and published as an ASAP article. Note that technical editing may introduce minor changes to the manuscript text and/or graphics which could affect content, and all legal disclaimers and ethical guidelines that apply to the journal pertain. ACS cannot be held responsible for errors or consequences arising from the use of information contained in these "Just Accepted" manuscripts.



ACS Publications
High quality. High impact.

Evidence of Catalase Mimetic Activity in Ce³⁺/Ce⁴⁺ Doped Bioactive Glasses

Valentina Nicolini¹, Elisa Gambuzzi¹, Gianluca Malavasi^{1,*}, Ledi Menabue¹, Maria Cristina Menziani¹,
Gigliola Lusvardi¹, Alfonso Pedone^{1,*}, Francesco Benedetti^{2,3}, Paola Luches^{3,*}, Sergio D’Addato^{2,3},
Sergio Valeri^{2,3}

¹ *Department of Chemical and Geological Sciences, University of Modena and Reggio Emilia, Via
Campi 183, 41125 Modena, Italy*

² *Department of Physical, Information and Mathematical Sciences, University of Modena and Reggio
Emilia, Via Campi 213/a, 41125 Modena, Italy*

³ *Istituto Nanoscienze – CNR, Via Campi 213/a, 41125 Modena, Italy*

*Corresponding authors:

Gianluca Malavasi

Alfonso Pedone

Paola Luches

Email: gmalavasi@unimore.it

Email: alfonso.pedone@unimore.it

Email: paola.luches@unimore.it

Phone: +39 059 2055041

Phone: +39 059 2055043

Phone: +39 059 2055313

Fax: +39 059 373543

Fax: +39 059 2055235

Abstract.

The ability of Ce-containing bioactive glasses to inhibit oxidative stress in terms of reduction of hydrogen peroxide, by mimicking the catalase enzyme activity is demonstrated here for the first time.

The antioxidant properties of three bioactive glasses containing an increasing amount of CeO_2 have been evaluated by following the degradation of hydrogen peroxide with time after immersion in H_2O_2 aqueous solutions with different concentration. XPS and UV-Vis measurements allowed us to determine the $\text{Ce}^{3+}/\text{Ce}^{4+}$ ratio in the bulk and on the glass surface, and to correlate it with the ability of the samples to show catalase mimetic activity. Interestingly, we have found that the bioactive glass with composition $23.2\text{Na}_2\text{O}-25.7\text{CaO}-43.4\text{SiO}_2-2.4\text{P}_2\text{O}_5-5.3\text{CeO}_2$ immersed in 0.1 M H_2O_2 aqueous solution is able to degrade 90% of it in one week. The reduction in bioactivity of the glasses with increasing CeO_2 content is here rationalized in terms of a lower amount of phosphate groups available for the hydroxyapatite layer formation, after binding with cerium ions. In fact, classical molecular dynamics simulations revealed that the addition of CeO_2 leads to the formation of cerium phosphate rich regions. The formation of an insoluble CePO_4 crystalline phase is also observed by XRD analysis after thermal treatment of the glass samples.

Keywords. Cerium, biomaterials, antioxidant properties, molecular dynamics, XRD, UV.

1. Introduction

In the field of biomaterial implantation, the so-called surgical stress response is a well-defined physiological mechanism that involves, during and after surgical procedures, the activation of inflammatory, endocrine, metabolic and immunologic mediators.¹⁻³

Surgical stress also includes the occurrence of oxidative stress, with production of reactive oxygen or nitrogen species that may overwhelm the defense systems of the organism. It has been demonstrated that the administration of antioxidants results in improved organ function, shortened convalescence, reduced morbidity and mortality occurring in the surgical stress response.^{4,5}

In this context, biomaterials that can contrast the effects of oxidative stress and inhibit excessive reactive oxygen species generation in a sustained manner may be a useful tool for therapies that target these medical problems.

Among biomaterials, bioactive glasses are widely used in bone defect reparation because they spontaneously bond and integrate with both soft and hard (bone) tissues in the living body.⁶ In fact, when bioactive glasses are implanted and in contact with biological fluids, a rapid formation of a thin hydroxycarbonate-apatite layer occurs on the surface of the material, enhancing living bone tissue regeneration.⁷ Since the early 1970s, when the first Bioglass[®] (45S5 glass: 24.5% Na₂O-24.5% CaO-45.0% SiO₂-6% P₂O₅ by weight)⁸ was synthesized, glasses of many different compositions have been studied to improve the material properties.⁹⁻¹³ For example, by varying the chemical nature and concentration of metal oxides, new important biological properties have been added, tailoring the glass to specific clinical applications.¹⁴⁻²¹

The design of bioactive glasses able to prevent oxidative stress after implantation would shorten the convalescence and reduce the amount of anti-inflammatory medications administered to patients. Moreover, the use of bioactive glasses able to act as antioxidant can be helpful in the management of osteoporosis.²²

In the recent years, it has been shown that nanoparticles of cerium oxide,^{23–28} RuO_2 ,²⁹ Fe_3O_4 ,²⁹ and Co_3O_4 ³⁰ are able to catalyze the decomposition of hydrogen peroxide (H_2O_2) into water and oxygen mimicking the catalase enzyme action. The role of the latter is very important, since it protects cells from oxidative stress caused by reactive oxygen species.^{31,32}

The ability of these nanoparticles to act against oxidative stress is closely related to the ability of the metal to present two oxidation states. For example, nanoparticles of ceria, CeO_2 (nanoceria), present oxygen vacancies associated to the presence of Ce^{3+} on the surface. Their surface exhibits a high $\text{Ce}^{3+}/\text{Ce}^{4+}$ ratio, whereas bulk CeO_2 is characterized by a low $\text{Ce}^{3+}/\text{Ce}^{4+}$ ratio.^{30,33} Thus, the redox properties of nanoceria determine its ability to protect tissues against oxidative stress.^{34–37}

In this scenario, we will investigate the possibility to imprint catalase mimetic activity to Ce-doped bioactive glasses.³⁸ Characterization of magnetic, optical and structural properties will be carried out both with experimental and computational methods. The latter approach will allow us to get a detailed description of the medium-range structural arrangement (~ 5 Å) of glasses and to correlate it with macroscopic properties. To the best of our knowledge, the ability of Ce-containing bioactive glasses to inhibit oxidative stress in terms of reduction of hydrogen peroxide will be demonstrated here for the first time. A relationship between antioxidant and bioactivity properties will also be discussed.

2. Experimental section

2.1 Preparation of glass powders.

Three different glasses containing 1.2%, 3.6% and 5.3% of CeO₂ (molar composition) were synthesized *via* melting procedure starting from the composition of the 45S5 Bioglass[®] (named hereafter BG), following the procedure describe in ref.³⁸

The nominal and effective molar composition of each sample is reported in Table 1. A BG sample was also prepared as reference. Samples were prepared by mixing reagent grade SiO₂, Na₂CO₃, CaCO₃, Na₃PO₄·12H₂O and CeO₂ in a glass beaker. Then each batch was put into a platinum crucible and melted in an electric oven. Heating ramp was set to 15°C/min up to 1000°C and 8°C/min up to 1350°C. Samples were maintained at this temperature for 2 hours, to ensure an optimal melting and mixing of all the oxides, and finally quenched at room temperature on a graphite plate. All the synthesized specimens were milled and sieved to obtain glass powders with particles in the range of 250-500µm.

2.2 Characterization of glasses

ICP measurements. The effective composition of each sample as quenched (AQ) was determined after dissolution by the Perkin Elmer Optima 4200DV inductive coupled plasma – optical emission spectrometer (ICP-OES), equipped with ultrasonic nebulizer CETAC useful for trace elements.

UV-Vis spectroscopy. To gain a qualitative estimation of the Ce⁴⁺ contained in the samples, UV-Vis analyses were performed on the as quenched powders. Spectra were acquired by using the HP8452 UV-Vis spectrometer in the 200-850 nm range for all samples. The diffuse reflectance technique with a BaSO₄ plate as reflectance standard was used.

X-Ray Diffraction (XRD) characterization. Powders of the doped glasses were crystallized at 660°C for 2 hours, then they were analyzed in the (2Θ) 10°-50° range, by means of X-ray diffraction apparatus (the X'Pert PRO-PANAnalytical) equipped with Ni-filtered Cu K_α radiation (λ = 1.54060 Å).

X-Ray Photoelectron Spectroscopy (XPS). XPS was used to obtain quantitative information on the relative amount of Ce³⁺ and Ce⁴⁺ on the surface of the samples. XPS spectra were collected at normal

emission using a hemispherical electron analyzer and Al K_{α} photons as the exciting probe. Due to the insulating nature of the samples, the XPS spectra were affected by charging effects, which resulted in a shift of the binding energy of the photoemission peaks. The shift ranges between 4.6 and 5.5 eV in the different samples. To account for this effect, the binding energy of each Ce 3d XPS spectrum was corrected by subtracting the difference between the binding energy of the 1s peak of adventitious carbon measured on the sample and the reference value of 285 eV.³⁹ In spite of the low concentration of Ce contained on the surface of the investigated samples, we managed to measure Ce 3d XPS spectra with an acceptable signal to noise ratio using long acquisition times (approximately 1 hour for the Ce 3d spectrum). The spectra were fit following a well established procedure, using three spin-orbit split doublets related to Ce^{4+} ionic species and two doublets related to Ce^{3+} ionic species.^{40–43} The spin-orbit splitting and branching ratio of each component and the differences in binding energy between the components were fixed to the values in ref.^{40–43} The Lorentzian and Gaussian width of the individual components were kept as close as possible to the values used in previous works on cerium oxide films with different degree of oxidation.^{41–43} In the fitting of the different spectra shown in this work the area of the peaks and a quadratic background were the only free parameters, while the binding energy, spin orbit splitting, branching ratio, widths and step of the Shirley type background for all components were fixed. The concentration of each ionic species was obtained from the relative weight of the area of its components compared to the total area of all Ce 3d components. It has to be noted that the accuracy of the concentration of the two Ce ionic species obtained in this way is not very high, but the considerations made in the following are mainly based on the evolution of their values in the different samples/conditions, which are considered to be reliable.^{40–43} Given the limited probing depth of the XPS technique, the information obtained can be related only to the first few nanometers below the surface of the investigated samples.

Molecular dynamic simulation. Classical MD simulations of the BG, BG_1.2Ce, BG_3.6Ce and BG_5.3Ce glasses were performed by means of the DL_POLY[®] package⁴⁴ employing a well-established melt-quench computational protocol.⁴⁵

In this approach, an initial random configuration containing about 10,000 atoms enclosed in a periodic cubic box with the experimental density is melted at 3200 K and then cooled down to 300 K at a nominal cooling rate of 5 K ps⁻¹. The resulting glass structures have been subjected to a final NVT trajectory of 0.3 ns; and the structural analysis was performed on 1001 configurations sampled at regular intervals during the last 0.2 ns of MD trajectory. The Ce⁴⁺/Ce³⁺ ratio of each glass composition was fixed accordingly to experimental findings. The interatomic forces acting between the constituting ions have been described by using a shell model force field able to accurately reproduce the short and medium range structure of multicomponent oxide glasses.⁴⁶⁻⁵³ In this model, cations are represented by rigid points bearing full formal charges (Si⁴⁺, P⁵⁺, Ca²⁺, Ce³⁺, Ce⁴⁺ etc...), whereas anions are split in a massless shell of charge -Y and a massive core of charge Z (Z+Y is the total atomic charge; -2 for O ions), which are coupled by a harmonic spring potential. The oxygen shell interacts with the Si⁴⁺, P⁵⁺, Ce³⁺, Ce⁴⁺, Ca²⁺ and Na⁺ cations through a Buckingham term, and coulomb forces act between all species bearing a formal charge, in the Born Mayer model. Three-body screened harmonic potentials have been employed to control the O-Si-O and O-P-O angles, for favoring tetrahedral coordination. Therefore, in the shell model the polarizability of oxygen is straightforwardly included, and it is also environment dependent due to the forces acting on the oxygen shell by the other ions. This allows for a better glass structure relaxation during quenching and leads to glasses with improved medium-range structures with respect to those generated by using the rigid ion model.⁵⁴ A detailed description of the force-field functional forms as well as the complete list of parameters is reported in refs.^{46,47,50}

2.3 Catalase mimetic activity tests

In order to verify whether glasses containing CeO_2 show catalase mimetic activity, the powder samples were soaked, under continuous stirring, in solutions of H_2O_2 at concentrations 1 M and 0.1 M.³⁴ The soaking time was set to 1, 2, 4 hours, 1, 4 and 7 days. In all the samples, a constant glass mass/solution volume ratio of 5 mg/ml was maintained. After soaking, the specimens were filtered; the powders were dried overnight at 60°C, whereas the solutions were titrated by KMnO_4 to determine the residual H_2O_2 . Before titration, pH of each solution was measured and the release of cerium from the specimens was determined by inductive coupled plasma – mass spectrometer (ICP-MS).

The powders were analyzed by UV-Vis spectroscopy (range 250-650 nm) and XPS in order to obtain qualitative and quantitative information about the $\text{Ce}^{3+}/\text{Ce}^{4+}$ ratio.

3. Results

3.1 Glass characterization.

ICP measurements. The effective compositions obtained by ICP analysis are reported in Table 1, together with the nominal ones. Notwithstanding small discrepancies are observed between the nominal and effective compositions, the ratios between the base constituent of the Ce-doped BGs are very similar to the ratios in the original Bioglass[®] 45S5.

UV-Vis spectroscopy. To gather qualitative information about the oxidation state of cerium contained in the glasses, UV-Vis measurements were performed. CeO_2 and $\text{Ce}(\text{NO}_3)_3 \cdot 6\text{H}_2\text{O}$ were used as references to precisely identify the absorption wavelengths of Ce^{3+} and Ce^{4+} respectively. Figure 1 shows that $\text{Ce}(\text{NO}_3)_3 \cdot 6\text{H}_2\text{O}$ present a broad peak between 250-350 nm (Figure 1), whereas CeO_2 shows two peaks, one in the range of 250-300 nm and one around 380 nm, in good agreement with previous stud-

ies.^{55–57} By considering that CeO_2 always carries a small portion of Ce_2O_3 on the surface, it is possible to assign the peak at 250–300 nm to Ce^{3+} and the peak at 350–400 nm at Ce^{4+} .

The BG sample shows a peak at 270 nm, that is the characteristic absorption wavelength of soda-lime-silicate glass.⁵⁸ Spectra of Ce-doped glasses show very broad peaks between 250–400 nm; thus, both Ce^{3+} and Ce^{4+} should be present in our specimens. Furthermore, the intensity of absorption between 400 and 600 nm is directly proportional to the content of CeO_2 in the sample composition, suggesting an increase in the quantity of Ce^{4+} .

XRD characterization. Previous investigations^{59,60} revealed that after heat treatment the BG sample crystallizes through the formation of a cyclo-silicate ($\text{Na}_2\text{CaSi}_2\text{O}_6$, JCPDS 77-2189) and a mixed Na-Ca ortho-phosphate ($\beta\text{-NaCaPO}_4$, JCPDS 76-1456). Figure 2 reports the XRD diffraction patterns before and after heat treatment of the Ce-containing BG samples investigated here. The patterns show peaks characteristic of three different phases: $\text{Na}_2\text{CaSi}_2\text{O}_6$ (JCPDS 77-2189), CePO_4 (JCPDS 32-199) and CeO_2 (JCPDS 34-0394). The presence of CePO_4 (JCPDS 32-199) and CeO_2 (JCPDS 34-0394) phases is strictly related to the Ce-content in the glasses, in fact the intensity of the peaks attributed to these phases increases passing from 1.2% CeO_2 to 5.3% CeO_2 , however in BG_1.2Ce crystallized sample only the peak attributed to CeO_2 was observed. Interestingly, Ce-containing glasses do not present the crystalline phase $\beta\text{-NaCaPO}_4$ detected in our previous work in BG sample in addition to $\text{Na}_2\text{CaSi}_2\text{O}_6$ crystals⁶¹, suggesting that the PO_4^{3-} structural units tend to attract cerium ions instead of sodium and calcium and favors the formation of CePO_4 instead of $\beta\text{-NaCaPO}_4$.

XPS. Figure 3 shows the Ce 3d XPS spectra measured on BG_5.3Ce, BG_3.6Ce and BG_1.2Ce AQ sample after Shirley-type background subtraction. All of the spectra in Figure 3 contain mainly features attributed to Ce^{3+} , although the individual peak around 916.5 eV, attributed to Ce^{4+} , has a non-negligible intensity in all samples. This evidence confirms that cerium contained in the glasses is always present in

both its oxidation states, as already observed by UV-Vis and magnetic susceptibility measurements. The fitting of the Ce 3d XPS spectra allowed a quantitative evaluation of the ratio between the two Ce ionic species on the glass surface. The $\text{Ce}^{3+}/\text{Ce}^{4+}$ ratio obtained for the AQ glass surface is 3.2 ± 0.2 for BG_5.3Ce, 2.8 ± 0.3 for BG_3.6Ce and 3.3 ± 0.5 for BG_1.2Ce. As expected, the $\text{Ce}^{3+}/\text{Ce}^{4+}$ ratio does not change significantly in samples with different Ce concentration.

Molecular dynamic simulations. An important structural feature related to the dissolution of ions in the physiological fluids is their coordination numbers $\text{CN}_{\text{X-Y}}$, that is, the number of neighbors of species Y in the first coordination shell of a given atom X. Table 2 reports the $\text{CN}_{\text{X-O}}$ of all the cations in the investigated glasses. As expected, both silicon and phosphorus ions are four-coordinated and their coordination numbers are not influenced by the addition of Ce ions.

On average, Ce^{3+} is coordinated by 6.5-6.6 non-bridging oxygens (NBOs) in all glasses, whereas Ce^{4+} is surrounded by about 7.0 NBOs, in agreement with previous MD investigations^{50,62,63} and EXAFS measurements^{64,65} on phosphate glasses. The coordination of cerium by NBOs only means that Ce acts as modifier cation that strongly competes for NBOs coordination with Na and Ca ions.

The latter are both coordinated by about 5.8 oxygens in the BG glass in agreement with previous investigations,⁶⁶⁻⁷⁰ but whereas the CN of Ca ions remains constant, the one of Na ions slightly increases to 6 with the CeO_2 content. The number of NBOs and bridging oxygen (BOs) atoms coordinated to Ca remains essentially constant in the four compositions, whereas a depletion of BO and an increment of NBO are observed around Na cations upon CeO_2 addition.

To investigate the effect of CeO_2 on the glass polymerization, the Q^n distributions (Q^n stands for 4-coordinated network former ion bonded to n bridging oxygens) of Si and P extracted from the MD trajectory for the BG, BG_1.2Ce, BG_3.6Ce and BG_5.3Ce glasses are listed in Table 3.

The cation-cation coordination numbers (CN_{X-Y}) computed by integrating the first peak of the corresponding pair distribution functions provides insights on the medium range order and chemical disorder of these glasses. Table 2 shows that the addition of CeO_2 oxide causes an increment in the number of Na ions in the second coordination sphere of Si: from 4.48, for BG glass, to 5.85 for BG_5.3Ce. At the same time, the number of Na surrounding P decreases from 6.05, for BG, to about 5.4-5.7 for Ce-containing compositions. The number of Ca ions around Si and P cations is less dependent on the addition of CeO_2 , though the second coordination sphere of P in BG_5.3Ce presents a lower number of Ca ions with respect to other glasses.

These data suggest that the Ce atoms tend to satisfy their own coordination requirements by using the NBOs belonging to PO_4^{3-} groups. Therefore, when inserted into the BG glass, Ce atoms push Na^+ ions away from P environment toward the silica network, which in turn depolymerizes in order to provide NBOs to Na^+ cations following the usual reaction $Si-O-Si + Na_2O \rightarrow 2SiONa$. The preference of Ce ions for phosphate groups is also witnessed by the comparison between the P/Si ratio around Ce ions in the MD models and the nominal ratio given by the glass composition (Table 2): the P/Si ratio in the second coordination sphere of Ce^{3+} ions is about 10 times higher than the nominal one (0.11). Figure 4 shows that P environment in BG glass (Figure 4.a) is rich in Na and Ca, whereas Ce ions replace part of Na and Ca in BG_5.3Ce (Figure 4.b). The structural differences are evident also in terms of silica network depolymerization: BG glass (Figure 4.c) presents a more polymerized structure, where both Ca and Na are allocated close to phosphate tetrahedra, while BG_5.3Ce glass (Figure 4.d) exhibits a highly depolymerized network with a prevalence of Na ions in Si closest surroundings.

The $Q^n(Si)$ distributions for the four compositions and the corresponding network connectivity, NC, (average number of BOs per network-forming atom) are quite different to each other. Although, the Si distribution is always dominated by Q^2 chain species, a significant amount of chain-terminators, Q^1 , and

1 branched, Q^3 , species are also present in all glasses. The addition of CeO_2 leads to a more fragmented
2 network with the NC monotonically decreasing from 2.08 for the BG glass to 1.74 for BG_5.3Ce glass.
3

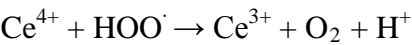
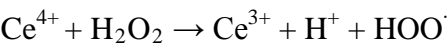
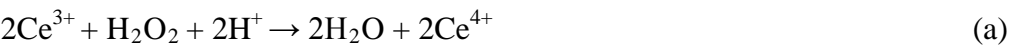
4
5 As for phosphorus, more than 76% of its ions are found in an orthophosphate (Q^0) environment in the
6 BG glass, but the amount of Q^0 species rapidly increases to 89% after the addition of only 5.3 mol% of
7 CeO_2 . The opposite trend is observed for $P(Q^1)$ sites, while the scant populations of $P(Q^2)$ sites does not
8 allow to speculate on its variation. However, it is evident that Ce has a strong impact on the medium
9 range order of these bioactive glasses.
10
11
12
13
14
15

16 17 **3.2 Catalase mimetic activity: in vitro tests and characterization after treatment.**

18
19
20 *Titration with $KMnO_4$.* Figure 5 reports the residual H_2O_2 concentrations after different soaking times
21 of the three Ce-containing samples in the original solutions with concentration of 0.1 M and 1.0 M. Both
22 trends highlight that the degradation of H_2O_2 is enhanced for glasses containing more CeO_2 . The results
23 show that the H_2O_2 degradations become apparent after 24 hours and proceed with the reaction time. In
24 particular, the most noticeable results were achieved with BG_3.6Ce and BG_5.3Ce samples soaked in
25 H_2O_2 solution for 168 hours with a reduction of around 64% and 90% of H_2O_2 concentration respec-
26 tively starting from H_2O_2 0.1 M and a reduction of around 17% and 35% respectively starting from
27 H_2O_2 1 M.
28
29
30
31
32
33
34
35
36
37

38
39 Stoichiometric calculations (not shown here) were carried out to determine the ratio between moles of
40 H_2O_2 decomposed after 168 hours (7 days) and moles of cerium contained in the samples. The resulting
41 H_2O_2/Ce ratios for BG_3.6Ce are 58 for H_2O_2 1 M and 22 for H_2O_2 0.1 M, while for BG_5.3Ce they
42 are 80 and 23, respectively. These ratios are underestimated since they were calculated by considering
43 all the amount of cerium contained in the samples, neglecting that only the Ce ions on the surface
44 should be able to interact with the hydrogen peroxide. This demonstrates that the amount of H_2O_2 de-
45 stroyed is in large excess with respect to the quantity of cerium in agreement with a catalytic behavior of
46
47
48
49
50
51
52
53
54
55

the metal; indeed Ce^{3+} is able to reduce H_2O_2 to H_2O and, at the same time, Ce^{4+} is able to oxidize it first to HOO^\cdot and then to O_2 . Starting from these considerations, we confirm the model of reaction mechanism for the dismutation of hydrogen peroxide by cerium oxide nanoparticles proposed by Celardo et al.⁷¹ and summarized in the following:





Summing reactions a) and b) the result is reaction c):



that is the same reaction through which the catalase enzyme destroys the hydrogen peroxide.⁷²

UV-Vis spectroscopy. The UV-Vis spectra performed over the soaked samples at different time have been compared with the dried powders spectra in Figure 6. The sample without Ce showed an absorbance at λ lower than 350 nm. This is characteristic of soda-lime silicate glasses⁷³ while the Ce-containing glasses started to adsorb at higher λ (<500 nm). It is possible to observe that the peaks of soaked samples shift to higher wavelength (λ) with respect to the AQ samples, that is, toward the λ of Ce^{4+} adsorption (380-400 nm). Thus, it is reasonable to assume that during the soaking in hydrogen peroxide, the Ce^{3+} ions in the samples convert partially to the Ce^{4+} state. Moreover, the intensity of the ab-

sorption at 168 hours is often lower than the intensity at 96 hours, possibly indicating that some Ce^{4+} ions reconvert to Ce^{3+} due to the catalase mimetic activity of the glasses.

ICP-MS measurements. ICP-MS measurements were performed over each filtered solution to gather information over the cerium released in solution during the soaking. As expected, samples with greater content in Ce release more metal and the concentration of Ce in solution falls in the range between 20 ppb and 1.5 ppm for all the samples. Furthermore, the greatest concentrations were obtained when glasses were soaked in H_2O_2 1 M, which is more aggressive towards the specimens. Also the greatest value of cerium in solution (1.5 ppm) obtained is not enough to justify the high abatement of H_2O_2 reached by soaking the samples, hence cerium ions on the glass surfaces should play a main role in the reaction with the hydrogen peroxide in solution. This hypothesis is confirmed by the fact that no decomposition of H_2O_2 is detected after 7 days for a solution of 1.5 ppm of Ce-salts (with different $\text{Ce}^{3+}/\text{Ce}^{4+}$ ratio) in H_2O_2 1 M. It is important to highlight that since the release of cerium ions in the environment is ten times lower than the LD_{50} reported in literature for cerium ions (15 ppm) the bioactive glasses investigated should not lead to toxicity problems.⁷⁴ For the sake of completeness, we reported also the value of LD_{50} of cerium oxide, which is 1000 ppm, according to OSHA and ANSI.⁷⁵ Furthermore, Zhang et al. reported in a recent study⁷⁶ that concentration up to 40 ppm of nanoceria protect the bone marrow stromal cells (BMSC) from the oxidative stress, increasing their viability when H_2O_2 solution is added to the environment.

pH-measurement. The pH was also monitored during the in vitro tests. An increment from 6.1 to 9.2 was observed after 7 days for all the samples in 0.1 M H_2O_2 solution, whereas the pH value increased to 10.7 after 7 days for all the samples in 1 M H_2O_2 solution. This increment is a well-known phenomenon due to the exchange between Na^+ at the glass surface with H^+ from the solution occurring in the first step of the Hench's bioactivity mechanism.^{7,77}

XPS. The analysis of the Ce 3d spectra allowed obtaining quantitative information on the evolution of $\text{Ce}^{3+}/\text{Ce}^{4+}$ ratio in the BG_5.3Ce glass after different soaking times. Figure 7a and b report the Ce 3d spectra for the 1 M and 0.1 M H_2O_2 solutions after selected soaking times and their fitting. A clear evolution of the Ce 3d shape with soaking time can be observed. The full set of values of the $\text{Ce}^{3+}/\text{Ce}^{4+}$ ratio obtained from the fitting at the different soaking times is reported in Figure 7c. A decrease of the intensity of Ce 3d signal was observed for soaking times longer than 1 hour in 1 M H_2O_2 solution, resulting in a lower signal-to-noise ratio in the spectra acquired after 1 day soaking in 1 M H_2O_2 in spite of the relatively long acquisition time. After 7 days for both H_2O_2 concentrations, the Ce 3d signal was almost suppressed. The Ce surface concentration decrease after long soaking times is ascribed to the formation of precipitate substances as Ca-phosphate phases on the glass surface. The $\text{Ce}^{3+}/\text{Ce}^{4+}$ ratio on the glass surface decreases for short soaking times in the 1 M H_2O_2 solution and it subsequently increases, reaching a value close to 1 for longer times. In the 0.1 M H_2O_2 solution the $\text{Ce}^{3+}/\text{Ce}^{4+}$ decrease is more significant and it persists for longer times than in the 1 M solution.

4. Discussion

The characterization carried out on Ce-doped BGs confirms that cerium is present in the two common oxidation states $\text{Ce}^{3+}/\text{Ce}^{4+}$, both in the bulk and on the surface. XPS analysis determined a $\text{Ce}^{3+}/\text{Ce}^{4+}$ ratio in the range 1.6 - 3.1 for the studied glasses.

In a recent work, Pirmohamed *et al.*²³ compared the catalase mimetic activity of two kinds of Ce NPs with different $\text{Ce}^{3+}/\text{Ce}^{4+}$ ratios (6-26) and found the best results for systems with low ratios.

Our results are in agreement with these findings. In fact, we found that all glasses are able to reduce the H_2O_2 concentration. In particular, the BG_Ce5.3 glass presents the best catalytic rate, since it is able to degrade 31.7 μmol of H_2O_2 per min. For example, a sample of 250 mg was able to decompose in 168 h a number of H_2O_2 moles equals to 80 times the moles of cerium contained in the whole bulk sample.

This catalytic rate is higher than that found by Pirmohamed *et al.* (2.71 nmol of H₂O₂ per min)²³ probably because the tests were performed using different concentrations of both H₂O₂ (10 mM as maximum value in the previous work) and CeO₂ nanoparticles.

The ability of the glasses to act as catalysts is also highlighted by the trend of Ce³⁺/Ce⁴⁺ after the soaking in H₂O₂ solution reported in Figure 7a. The ratio shows a great variation at short time and it becomes more or less constant at longer time, suggesting a similar velocity of the two proposed reactions a) and b) at longer times. Moreover, at short soaking times (1-4 hours) a significant color change from light yellow to deep yellow-orange was observed indicating that Ce³⁺ (colorless) on the glass surface was oxidized to Ce⁴⁺ (yellow-orange)⁷⁸ by H₂O₂. The color of the sample remained the same in the rest of the observations. Therefore, it can be hypothesized that at short times reaction a) occurs at the glass surface, and, since the specific surface area of the sample is low, this process causes a low decomposition of H₂O₂. Instead, at longer times (>1 day) the catalytic cycle of reaction a) + b) starts, and the increment of specific surface area,⁷⁹ due to the partial dissolution of the glass, increases the rate of H₂O₂ decomposition since more Ce³⁺ and Ce⁴⁺ ions become available.

Interestingly, the glasses are active in a wide range of pH, from 6 to 9.2 and 10.7 as a function of H₂O₂ concentration and time. This is very important because it is the range of pH commonly reached in the fluids surrounding the implanted biomaterial.⁸⁰

The XRD analysis and MD results suggest the absence of CeO₂ nanocrystals in the glass matrix. Both techniques revealed that in the glass structure Ce ions and phosphate groups tend to aggregate forming Ce-phosphate rich zones. In view of this results we can ascribe the catalase mimetic activity to the simultaneous presence on the material surface of Ce³⁺ and Ce⁴⁺ sites, opening a new door on the development of inorganic materials exhibiting redox state-dependent mimetic enzyme activity.

From one hand, the increasing of CeO₂ content in the glass compositions enhances anti-oxidant ability, but from another hand, the bioactivity decreases (delay of hydroxyapatite formation) as reported by Leonelli *et al.*³⁸ The computational simulation of glass structures allowed us to relate this phenomenon with the medium-range order of the matrix. In fact, Ce atoms tend to allocate close to phosphate domains, preventing their release from the glass network, thus making them less available for the hydroxyapatite layer formation, or involving them in the formation of a stable, insoluble CePO₄ crystalline phase. Moreover, the introduction of CeO₂ in these glasses avoids the formation of calcium phosphate domains that can act as crystallization nuclei able to speed up the crystallization of Ca₃(PO₄)₂ on the glass surface and the formation of hydroxyapatite and could influence ions release.^{81,82,83} Therefore a good compromise between a high bioactivity level and an efficient catalase mimetic activity requires a proper adjustment of cerium oxide content in the glasses. An alternative way to obtain both good bioactivity and efficient catalytic activity could be the synthesis of the glasses through the sol-gel method.⁸⁴ Indeed, in a previous work Shruti *et al.* have verified that bioactive glasses obtained *via* sol-gel and doped with 3.5% mol cerium oxide do not show a substantial difference in bioactivity, compared to the undoped glass.²⁰ This is likely due to the fact that porous sol-gel glasses show higher bioactivity with respect to the glasses obtained by melting. Thus, it is possible that adding an amount greater than 3.5% to the sol-gel glasses, they could show both bioactivity and antioxidant properties.

5. Conclusions

1 In conclusion, we have demonstrated for the first time that it is possible to confer catalase mimetic ac-
2 tivity to bioactive glasses by adding CeO₂. This property is related to the simultaneous presence of Ce³⁺
3 and Ce⁴⁺ both in the bulk structure and on the surface with a ratio close to 3.
4
5
6

7 The structural information gained by XRD measurements and MD simulations showed that the intro-
8 duction of cerium has a strong impact on the medium range order of the glasses investigated, favoring
9 the formation of Ce-phosphate insoluble phases that increase the chemical durability. Thus, the em-
10 ployment of CeO₂-doped bioactive glasses could become a valid alternative to the addition of ceria na-
11 noparticles to biomaterials.
12
13
14
15
16
17
18
19
20
21
22
23
24
25
26
27
28
29
30
31
32
33
34
35
36
37

38 **Acknowledgment**

39 This work was supported by a grant from the University of Modena and Reggio Emilia entitled ‘The
40 role of cerium oxidation state in bioactive glasses used as biomaterials of 3rd generation’. Support by the
41 COST Action CM1104 ‘Reducible oxide chemistry, structure and functions’ is also acknowledged.
42
43
44
45
46
47
48
49
50
51
52
53
54
55
56
57
58
59
60

Supporting Information Available

Magnetic susceptibility data collected over the AQ samples. Table S1: The magnetic moment (μ_{eff}) of as quenched (AQ) samples. This material is available free of charge *via* the Internet at <http://pubs.acs.org/>.

Bibliographic References

- (1) Kinov, P.; Leithner, A.; Radl, R.; Bodo, K.; Khoshsorur, G.-A.; Schauenstein, K.; Windhager, R. Role of Free Radicals in Aseptic Loosening of Hip Arthroplasty. *J. Orthop. Res. Off. Publ. Orthop. Res. Soc.* **2006**, *24*, 55–62.
- (2) Gałęcka, E.; Jacewicz, R.; Mrowicka, M.; Florkowski, A.; Gałęcki, P. Antioxidative Enzymes--Structure, Properties, Functions. *Pol. Merkur. Lek. Organ Pol. Tow. Lek.* **2008**, *25*, 266–268.
- (3) Küçükakin, B.; Gögenur, I.; Reiter, R. J.; Rosenberg, J. Oxidative Stress in Relation to Surgery: Is There a Role for the Antioxidant Melatonin? *J. Surg. Res.* **2009**, *152*, 338–347.
- (4) Nathens, A. B.; Neff, M. J.; Jurkovich, G. J.; Klotz, P.; Farver, K.; Ruzinski, J. T.; Radella, F.; Garcia, I.; Maier, R. V. Randomized, Prospective Trial of Antioxidant Supplementation in Critically Ill Surgical Patients. *Ann. Surg.* **2002**, *236*, 814–822.
- (5) Berger, M. M.; Soguel, L.; Shenkin, A.; Revelly, J.-P.; Pinget, C.; Baines, M.; Chioloro, R. L. Influence of Early Antioxidant Supplements on Clinical Evolution and Organ Function in Critically Ill Cardiac Surgery, Major Trauma, and Subarachnoid Hemorrhage Patients. *Crit. Care* **2008**, *12*, R101.
- (6) Wilson, J.; Yli-Urpo, A.; Risto-Pekka, H. Bioactive Glasses: Clinical Applications. *An introduction to bioceramics*, 1993, 63–74.
- (7) Jones, J. R. Review of Bioactive Glass: From Hench to Hybrids. *Acta Biomater.* **2013**, *9*, 4457–4486.
- (8) Hench, L. L. Bioceramics. *J Am Ceram Soc* **1998**, *81*, 1705–1728.
- (9) Vallet-Regí, M.; Ruiz-Hernández, E. Bioceramics: From Bone Regeneration to Cancer Nanomedicine. *Adv. Mater.* **2011**, *23*, 5177–5218.
- (10) Izquierdo-Barba, I.; Vallet-Regí, M. Fascinating Properties of Bioactive Templated Glasses: A New Generation of Nanostructured Bioceramics. *Solid State Sci.* **2011**, *13*, 773–783.
- (11) Arcos, D.; Vallet-Regí, M. Sol–gel Silica-Based Biomaterials and Bone Tissue Regeneration. *Acta Biomater.* **2010**, *6*, 2874–2888.
- (12) Vallet-Regi, M.; Izquierdo-Barba, I.; Colilla, M. Structure and Functionalization of Mesoporous Bioceramics for Bone Tissue Regeneration and Local Drug Delivery. *Philos. Trans. R. Soc. Math. Phys. Eng. Sci.* **2012**, *370*, 1400–1421.
- (13) Xiang, Y.; Du, J. Effect of Strontium Substitution on the Structure of 45S5 Bioglasses. *Chem. Mater.* **2011**, *23*, 2703–2717.
- (14) Boyd, D.; Carroll, G.; Towler, M. R.; Freeman, C.; Farthing, P.; Brook, I. M. Preliminary Investigation of Novel Bone Graft Substitutes Based on Strontium–calcium–zinc–silicate Glasses. *J. Mater. Sci. Mater. Med.* **2009**, *20*, 413–420.
- (15) Lusvardi, G.; Malavasi, G.; Menabue, L.; Menziani, M. C.; Pedone, A.; Segre, U.; Aina, V.; Perardi, A.; Morterra, C.; Boccafroschi, F.; et al. Properties of Zinc Releasing Surfaces for Clinical Applications. *J. Biomater. Appl.* **2007**, *22*, 505–526.
- (16) Li, X.; Wang, X.; He, D.; Shi, J. Synthesis and Characterization of Mesoporous CaO–MO–SiO₂–P₂O₅ (M = Mg, Zn, Cu) Bioactive Glasses/composites. *J. Mater. Chem.* **2008**, *18*, 4103.
- (17) Fong, L.; Tan, K.; Tran, C.; Cool, J.; Scherer, M. A.; Elovaris, R.; Coyle, P.; Foster, B. K.; Rofe, A. M.; Xian, C. J. Interaction of Dietary Zinc and Intracellular Binding Protein Metallothionein in Postnatal Bone Growth. *Bone* **2009**, *44*, 1151–1162.
- (18) Hoppe, A.; Guldal, N. S.; Boccaccini, A. R. A Review of the Biological Response to Ionic Dissolution Products from Bioactive Glasses and Glass-Ceramics. *Biomaterials* **2011**, *32*, 2757–2774.

- (19) Sánchez-Salcedo, S.; Shruti, S.; Salinas, A. J.; Malavasi, G.; Menabue, L.; Vallet-Regí, M. In Vitro Antibacterial Capacity and Cytocompatibility of SiO_2 – CaO – P_2O_5 Meso-Macroporous Glass Scaffolds Enriched with ZnO. *J. Mater. Chem. B* **2014**, *2*, 4836.
- (20) Shruti, S.; Salinas, A. J.; Malavasi, G.; Lusvardi, G.; Menabue, L.; Ferrara, C.; Mustarelli, P.; Vallet-Regí, M. Structural and in Vitro Study of Cerium, Gallium and Zinc Containing Sol–gel Bioactive Glasses. *J. Mater. Chem.* **2012**, *22*, 13698.
- (21) Gerhardt, L.-C.; Boccaccini, A. R. Bioactive Glass and Glass-Ceramic Scaffolds for Bone Tissue Engineering. *Materials* **2010**, *3*, 3867–3910.
- (22) Arcos, D.; Boccaccini, A. R.; Bohner, M.; Díez-Pérez, A.; Epple, M.; Gómez-Barrena, E.; Herrera, A.; Planell, J. A.; Rodríguez-Mañas, L.; Vallet-Regí, M. The Relevance of Biomaterials to the Prevention and Treatment of Osteoporosis. *Acta Biomater.* **2014**, *10*, 1793–1805.
- (23) Pirmohamed, T.; Dowding, J. M.; Singh, S.; Wasserman, B.; Heckert, E.; Karakoti, A. S.; King, J. E. S.; Seal, S.; Self, W. T. Nanoceria Exhibit Redox State-Dependent Catalase Mimetic Activity. *Chem. Commun.* **2010**, *46*, 2736.
- (24) Dowding, J. M.; Das, S.; Kumar, A.; Dosani, T.; McCormack, R.; Gupta, A.; Sayle, T. X. T.; Sayle, D. C.; von Kalm, L.; Seal, S.; et al. Cellular Interaction and Toxicity Depend on Physicochemical Properties and Surface Modification of Redox-Active Nanomaterials. *ACS Nano* **2013**, *7*, 4855–4868.
- (25) Das, M.; Patil, S.; Bhargava, N.; Kang, J.-F.; Riedel, L. M.; Seal, S.; Hickman, J. J. Auto-Catalytic Ceria Nanoparticles Offer Neuroprotection to Adult Rat Spinal Cord Neurons. *Biomaterials* **2007**, *28*, 1918–1925.
- (26) Karakoti, A. S.; Das, S.; Thevuthasan, S.; Seal, S. PEGylated Inorganic Nanoparticles. *Angew. Chem. Int. Ed.* **2011**, *50*, 1980–1994.
- (27) Karakoti, A.; Singh, S.; Dowding, J. M.; Seal, S.; Self, W. T. Redox-Active Radical Scavenging Nanomaterials. *Chem. Soc. Rev.* **2010**, *39*, 4422.
- (28) Gupta, A.; Das, S.; Seal, S. Redox-Active Nanoparticles in Combating Neurodegeneration. *Nanomed.* **2014**, *9*, 2725–2728.
- (29) Deng, H.; Shen, W.; Peng, Y.; Chen, X.; Yi, G.; Gao, Z. Nanoparticulate Peroxidase/Catalase Mimetic and Its Application. *Chem. - Eur. J.* **2012**, *18*, 8906–8911.
- (30) Mu, J.; Zhang, L.; Zhao, M.; Wang, Y. Co_3O_4 Nanoparticles as an Efficient Catalase Mimic: Properties, Mechanism and Its Electrocatalytic Sensing Application for Hydrogen Peroxide. *J. Mol. Catal. Chem.* **2013**, *378*, 30–37.
- (31) Brioukhanov, A. L.; Netrusov, A. I. Catalase and Superoxide Dismutase: Distribution, Properties, and Physiological Role in Cells of Strict Anaerobes. *Biochem. Mosc.* **2004**, *69*, 949–962.
- (32) Ohno, Y.; Gallin, J. I. Diffusion of Extracellular Hydrogen Peroxide into Intracellular Compartments of Human Neutrophils. Studies Utilizing the Inactivation of Myeloperoxidase by Hydrogen Peroxide and Azide. *J. Biol. Chem.* **1985**, *260*, 8438–8446.
- (33) Campbell, C. T. CHEMISTRY: Oxygen Vacancies and Catalysis on Ceria Surfaces. *Science* **2005**, *309*, 713–714.
- (34) Heckert, E. G.; Karakoti, A. S.; Seal, S.; Self, W. T. The Role of Cerium Redox State in the SOD Mimetic Activity of Nanoceria. *Biomaterials* **2008**, *29*, 2705–2709.
- (35) Karakoti, A. S.; Singh, S.; Kumar, A.; Malinska, M.; Kuchibhatla, S. V. N. T.; Wozniak, K.; Self, W. T.; Seal, S. PEGylated Nanoceria as Radical Scavenger with Tunable Redox Chemistry. *J. Am. Chem. Soc.* **2009**, *131*, 14144–14145.
- (36) Deshpande, S.; Patil, S.; Kuchibhatla, S. V.; Seal, S. Size Dependency Variation in Lattice Parameter and Valency States in Nanocrystalline Cerium Oxide. *Appl. Phys. Lett.* **2005**, *87*, 133113.

- (37) Korsvik, C.; Patil, S.; Seal, S.; Self, W. T. Superoxide Dismutase Mimetic Properties Exhibited by Vacancy Engineered Ceria Nanoparticles. *Chem. Commun.* **2007**, 1056.
- (38) Leonelli, C.; Lusvardi, G.; Malavasi, G.; Menabue, L.; Tonelli, M. Synthesis and Characterization of Cerium-Doped Glasses and in Vitro Evaluation of Bioactivity. *J. Non-Cryst. Solids* **2003**, *316*, 198–216.
- (39) Swift, P. Adventitious Carbon? the Panacea for Energy Referencing? *Surf. Interface Anal.* **1982**, *4*, 47–51.
- (40) Romeo, M.; Bak, K.; El Fallah, J.; Le Normand, F.; Hilaire, L. XPS Study of the Reduction of Cerium Dioxide. *Surf. Interface Anal.* **1993**, *20*, 508–512.
- (41) Skála, T.; Šutara, F.; Škoda, M.; Prince, K. C.; Matolín, V. Palladium Interaction with CeO₂, Sn–Ce–O and Ga–Ce–O Layers. *J. Phys. Condens. Matter* **2009**, *21*, 055005.
- (42) Luches, P.; Pagliuca, F.; Valeri, S. Morphology, Stoichiometry, and Interface Structure of CeO₂ Ultrathin Films on Pt(111). *J. Phys. Chem. C* **2011**, *115*, 10718–10726.
- (43) Luches, P.; Pagliuca, F.; Valeri, S. Structural and Morphological Modifications in Thermally Reduced Cerium Oxide Ultrathin Epitaxial Films on Pt(111). *Phys. Chem. Chem. Phys.* **2014**.
- (44) Smith, W.; Forester, T. R. DL_POLY_2.0: A General-Purpose Parallel Molecular Dynamics Simulation Package. *J. Mol. Graph.* **1996**, *14*, 136–141.
- (45) Pedone, A. Properties Calculations of Silica-Based Glasses by Atomistic Simulations Techniques: A Review. *J. Phys. Chem. C* **2009**, *113*, 20773–20784.
- (46) Tilocca, A. Short- and Medium-Range Structure of Multicomponent Bioactive Glasses and Melts: An Assessment of the Performances of Shell-Model and Rigid-Ion Potentials. *J. Chem. Phys.* **2008**, *129*, 084504.
- (47) Pedone, A.; Malavasi, G.; Menziani, M. C. Computational Insight into the Effect of CaO/MgO Substitution on the Structural Properties of Phospho-Silicate Bioactive Glasses. *J. Phys. Chem. C* **2009**, *113*, 15723–15730.
- (48) Malavasi, G.; Pedone, A.; Menziani, M. C. Study of the Structural Role of Gallium and Aluminum in 45S5 Bioactive Glasses by Molecular Dynamics Simulations. *J. Phys. Chem. B* **2013**, *117*, 4142–4150.
- (49) Gambuzzi, E.; Pedone, A.; Menziani, M. C.; Angeli, F.; Caurant, D.; Charpentier, T. Probing Silicon and Aluminium Chemical Environments in Silicate and Aluminosilicate Glasses by Solid State NMR Spectroscopy and Accurate First-Principles Calculations. *Geochim. Cosmochim. Acta* **2014**, *125*, 170–185.
- (50) Gambuzzi, E.; Pedone, A. On the Structure of Ce-Containing Silicophosphate Glasses: A Core-shell Molecular Dynamics Investigation. *Phys Chem Chem Phys* **2014**, *16*, 21645–21656.
- (51) Ainsworth, R. I.; Di Tommaso, D.; Christie, J. K.; de Leeuw, N. H. Polarizable Force Field Development and Molecular Dynamics Study of Phosphate-Based Glasses. *J. Chem. Phys.* **2012**, *137*, 234502.
- (52) Pedone, A.; Gambuzzi, E.; Menziani, M. C. Unambiguous Description of the Oxygen Environment in Multicomponent Aluminosilicate Glasses from ¹⁷O Solid State NMR Computational Spectroscopy. *J. Phys. Chem. C* **2012**, *116*, 14599–14609.
- (53) Pedone, A.; Gambuzzi, E.; Malavasi, G.; Menziani, M. C. First-Principles Simulations of the ²⁷Al and ¹⁷O Solid-State NMR Spectra of the CaAl₂Si₃O₁₀ Glass. *Theor. Chem. Acc.* **2012**, *131*.
- (54) Tilocca, A.; de Leeuw, N.; Cormack, A. Shell-Model Molecular Dynamics Calculations of Modified Silicate Glasses. *Phys. Rev. B* **2006**, *73*.

- (55) Assefa, Z.; Haire, R. G.; Caulder, D. L.; Shuh, D. K. Correlation of the Oxidation State of Cerium in Sol-gel Glasses as a Function of Thermal Treatment via Optical Spectroscopy and XANES Studies. *Spectrochim. Acta. A. Mol. Biomol. Spectrosc.* **2004**, *60*, 1873–1881.
- (56) Paje, S. ; García, M. ; Villegas, M. ; Llopis, J. Cerium Doped Soda-Lime-Silicate Glasses: Effects of Silver Ion-Exchange on Optical Properties. *Opt. Mater.* **2001**, *17*, 459–469.
- (57) Xia, C.; Hu, C.; Chen, P.; Wan, B.; He, X.; Tian, Y. Magnetic Properties and Photoabsorption of the Mn-Doped CeO₂ Nanorods. *Mater. Res. Bull.* **2010**, *45*, 794–798.
- (58) Silverstein, R. M.; Webster, F. X.; Kiemle. *Spectrometric Identification of Organic Compounds*; Wiley Global Education, 2005.
- (59) Linati, L.; Lusvardi, G.; Malavasi, G.; Menabue, L.; Menziani, M. C.; Mustarelli, P.; Segre, U. Qualitative and Quantitative Structure–Property Relationships Analysis of Multicomponent Potential Bioglasses. *J. Phys. Chem. B* **2005**, *109*, 4989–4998.
- (60) Aina, V.; Cerrato, G.; Martra, G.; Bergandi, L.; Costamagna, C.; Ghigo, D.; Malavasi, G.; Lusvardi, G.; Menabue, L. Gold-Containing Bioactive Glasses: A Solid-State Synthesis to Produce Alternative Biomaterials for Bone Implantations. *J. R. Soc. Interface* **2013**, *10*, 20121040–20121040.
- (61) Lusvardi, G.; Malavasi, G.; Menabue, L.; Menziani, M. C.; Pedone, A.; Segre, U. A Computational Tool for the Prediction of Crystalline Phases Obtained from Controlled Crystallization of Glasses. *J. Phys. Chem. B* **2005**, *109*, 21586–21592.
- (62) Du, J.; Kokou, L.; Rygel, J. L.; Chen, Y.; Pantano, C. G.; Woodman, R.; Belcher, J. Structure of Cerium Phosphate Glasses: Molecular Dynamics Simulation: Structure of Cerium Phosphate Glasses. *J. Am. Ceram. Soc.* **2011**, *94*, 2393–2401.
- (63) Kokou, L.; Du, J. Short- and Medium-Range Structures of Cerium Aluminophosphate Glasses: A Molecular Dynamics Study. *J. Non-Cryst. Solids* **2014**, *403*, 67–79.
- (64) Brow, R. K.; Wittenauer, A. K. RARE EARTH COORDINATION ENVIRONMENTS IN ULTRAPHOSPHATE GLASSES. **2002**, *13*, 95–100.
- (65) Mountjoy, G. Molecular Dynamics, Diffraction and EXAFS of Rare Earth Phosphate Glasses Compared with Predictions Based on Bond Valence. *J. Non-Cryst. Solids* **2007**, *353*, 2029–2034.
- (66) Malavasi, G.; Menziani, M. C.; Pedone, A.; Civalleri, B.; Corno, M.; Ugliengo, P. A Computational Multiscale Strategy to the Study of Amorphous Materials. *Theor. Chem. Acc.* **2007**, *117*, 933–942.
- (67) Corno, M.; Pedone, A. Vibrational Features of Phospho-Silicate Glasses: Periodic B3LYP Simulations. *Chem. Phys. Lett.* **2009**, *476*, 218–222.
- (68) Tilocca, A.; Cormack, A. N.; de Leeuw, N. H. The Structure of Bioactive Silicate Glasses: New Insight from Molecular Dynamics Simulations. *Chem. Mater.* **2007**, *19*, 95–103.
- (69) Christie, J. K.; Pedone, A.; Menziani, M. C.; Tilocca, A. Fluorine Environment in Bioactive Glasses: *ab Initio* Molecular Dynamics Simulations. *J. Phys. Chem. B* **2011**, *115*, 2038–2045.
- (70) Gambuzzi, E.; Charpentier, T.; Menziani, M. C.; Pedone, A. Computational Interpretation of ²³Na MQMAS NMR Spectra: A Comprehensive Investigation of the Na Environment in Silicate Glasses. *Chem. Phys. Lett.* **2014**, *612*, 56–61.
- (71) Celardo, I.; Pedersen, J. Z.; Traversa, E.; Ghibelli, L. Pharmacological Potential of Cerium Oxide Nanoparticles. *Nanoscale* **2011**, *3*, 1411.
- (72) Robbins, S. L.; Kumar, V.; Cotran, R. S. *Robbins and Cotran Pathologic Basis of Disease*; Saunders/Elsevier: Philadelphia, PA, 2010.
- (73) Goodyear, J. K.; Lindberg, V. L. Low Absorption Float Glass for Back Surface Solar Reflectors. *Sol. Energy Mater.* **1980**, *3*, 57–67.

- (74) Bjondahl, K. Differences in Liver Weight, Mortality in Cerium-Treated Mice and ^{144}Ce Levels in Blood, Liver, Urine and Faeces at Various Intervals after Treatment with Nafenopin and Pregnenolone 16-Alpha-Carbonitrile (PCN). *Med. Biol.* **1976**, *54*, 454–460.
- (75) *Material Safety Data Sheet - According to OSHA and ANSI*; 2011.
- (76) Zhang, Q.; Ge, K.; Duan, J.; Chen, S.; Zhang, R.; Zhang, C.; Wang, S.; Zhang, J. Cerium Oxide Nanoparticles Protect Primary Mouse Bone Marrow Stromal Cells from Apoptosis Induced by Oxidative Stress. *J. Nanoparticle Res.* **2014**, *16*.
- (77) Hench, L. L. Bioceramics: From Concept to Clinic. *J. Am. Ceram. Soc.* **1991**, *74*, 1487–1510.
- (78) Xu, C.; Qu, X. Cerium Oxide Nanoparticle: A Remarkably Versatile Rare Earth Nanomaterial for Biological Applications. *NPG Asia Mater.* **2014**, *6*, e90.
- (79) Lusvardi, G.; Malavasi, G.; Menabue, L.; Aina, V.; Morterra, C. Fluoride-Containing Bioactive Glasses: Surface Reactivity in Simulated Body Fluids Solutions. *Acta Biomater.* **2009**, *5*, 3548–3562.
- (80) Hench, L. L.; Splinter, R. J.; Allen, W. C.; Greenlee, T. K. Bonding Mechanisms at the Interface of Ceramic Prosthetic Materials. *J. Biomed. Mater. Res.* **1971**, *5*, 117–141.
- (81) Fayon, F.; Duée, C.; Poumeyrol, T.; Allix, M.; Massiot, D. Evidence of Nanometric-Sized Phosphate Clusters in Bioactive Glasses As Revealed by Solid-State ^{31}P NMR. *J. Phys. Chem. C* **2013**, *117*, 2283–2288.
- (82) Camiré, C. L.; Gbureck, U.; Hirsiger, W.; Bohner, M. Correlating Crystallinity and Reactivity in an A-Tricalcium Phosphate. *Biomaterials* **2005**, *26*, 2787–2794.
- (83) Vallet-Regí, M.; Salinas, A. J.; Ramírez-Castellanos, J.; González-Calbet, J. M. Nanostructure of Bioactive Sol–Gel Glasses and Organic–Inorganic Hybrids. *Chem. Mater.* **2005**, *17*, 1874–1879.
- (84) Hench, L. L.; West, J. K. The Sol-Gel Process. *Chem. Rev.* **1990**, *90*, 33–72.

Tables

Table 1. Nominal and effective molar compositions (%) of the synthesized glasses obtained by three different measurements (\pm std. dev.).

Nominal	BG	BG_1.2Ce	BG_3.6Ce	BG_5.3Ce
CeO ₂	-	1.2	3.6	5.3
SiO ₂	46.2	45.6	42.5	43.4
Na ₂ O	24.3	24.0	24.4	23.2
CaO	26.9	26.6	27.0	25.7
P ₂ O ₅	2.6	2.6	2.5	2.4
Effective				
CeO ₂	-	1.0 \pm 0.1	3.2 \pm 0.2	5.1 \pm 0.4
SiO ₂	47.8 \pm 1.5	44.5 \pm 1.6	41.4 \pm 2.0	40.8 \pm 2.5
Na ₂ O	23.5 \pm 2.2	27.4 \pm 2.4	29.0 \pm 2.8	30.1 \pm 2.9
CaO	26.0 \pm 2.4	24.6 \pm 2.3	24.1 \pm 2.2	21.9 \pm 2.2
P ₂ O ₅	2.6 \pm 0.2	2.5 \pm 0.2	2.3 \pm 0.2	2.1 \pm 0.2

Table 2. Average coordination numbers for the first and second coordination shells; ratio of the number of P and Si around Ce^{3+} $((\text{P/Si})_{\text{Ce}^{3+}})$, Ce^{4+} $((\text{P/Si})_{\text{Ce}^{4+}})$ and in the glass structure $((\text{P/Si})_{\text{GLASS}})$.

$\text{CN}_{\text{X-O}}$	BG	BG_1.2Ce	BG_3.6Ce	BG_5.3Ce
First coordination shell ($\text{CN}_{\text{X-O}}$)				
Si-O	4.00	4.00	4.00	4.00
P-O	4.00	4.00	4.00	4.00
Ca-O	5.76	5.82	5.94	5.86
Ca-BO	0.47	0.46	0.54	0.45
Ca-NBO	5.29	5.31	5.40	5.41
Na-O	5.81	5.36	6.02	6.01
Na-BO	1.35	1.36	1.25	1.20
Na-NBO	4.46	4.55	4.77	4.81
Ce^{3+} -NBO*	---	6.53	6.62	6.57
Ce^{4+} -NBO*	---	7.00	7.08	6.98
Second coordination shell ($\text{CN}_{\text{X-Y}}$)				
Si-Na	4.48	5.01	5.00	5.85
Si-Ca	2.93	2.95	2.98	2.89
P-Na	6.05	5.76	5.39	5.68
P-Ca	3.63	3.68	3.68	3.30
P/Si				
$((\text{P/Si})_{\text{Ce}^{3+}})$	---	1.20	1.07	1.12
$((\text{P/Si})_{\text{Ce}^{4+}})$	---	0.25	1.37	1.09
$((\text{P/Si})_{\text{GLASS}})$	----	0.11	0.11	0.11

(*) Ce atoms are coordinated by NBOs only.

Table 3. Q^n distributions and network connectivity, NC (average number of BOs coordinating network forming atoms), of P and Si network former cations, calculated for the studied glasses by MD simulations.

	BG	BG_1.2Ce	BG_3.6Ce	BG_5.3Ce
Q ⁿ (Si) speciation (pop%)				
n=0	0.9	1.2	2.2	3.2
n=1	19.2	22.5	29.2	35.0
n=2	51.9	52.9	51.8	46.9
n=3	25.9	21.9	15.9	13.9
n=4	2.0	1.5	1.0	1.0
NC	2.09	2.00	1.84	1.74
Q ⁿ (P) speciation (pop%)				
n=0	76.7	77.7	85.3	89.4
n=1	22.2	21.2	14.7	10.1
n=2	1.1	1.1	0.0	0.6
NC	0.24	0.23	0.15	0.11

Figures

Figure 1. UV-Vis spectra of glass samples and standard substances containing Ce^{3+} (cerium nitrate hexa-hydrate) and Ce^{4+} (cerium dioxide).

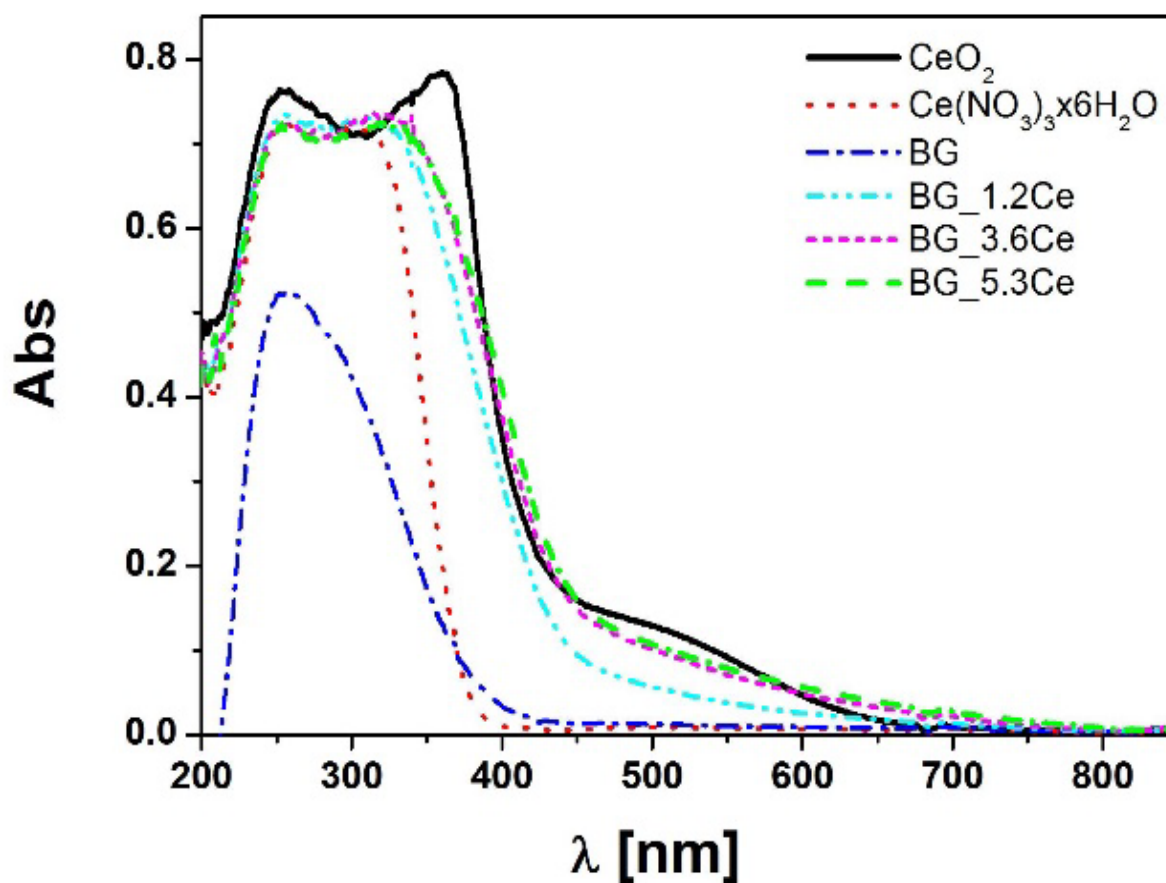


Figure 2. XRD spectra of BG_1.2Ce and BG_3.6Ce crystallized samples at 660°C for 2 hours. XRD spectra of BG_5.3Ce before (AQ) and after crystallization at 660°C for 2 hours. (the XRD spectrum of BG crystallized is reported in reference⁶⁰).

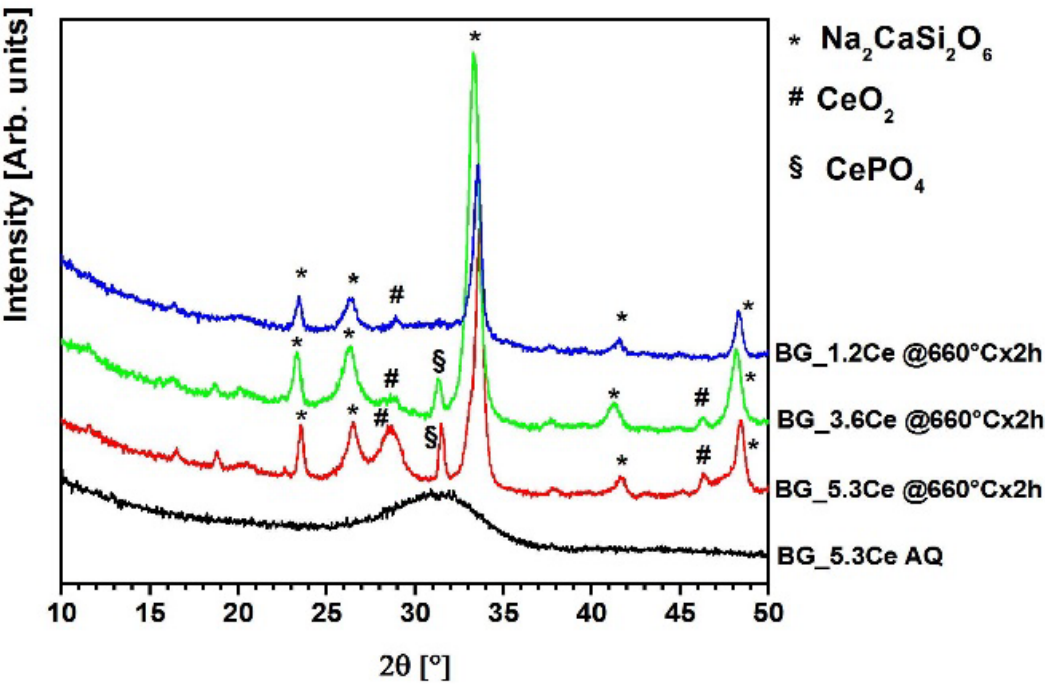


Figure 3. Ce 3d XPS spectra for BG_5.3Ce, BG_3.6Ce and BG_1.2Ce samples (red lines). The spectra are shown after Shirley-type background subtraction. For each peak the fitting curve is also shown (black lines).

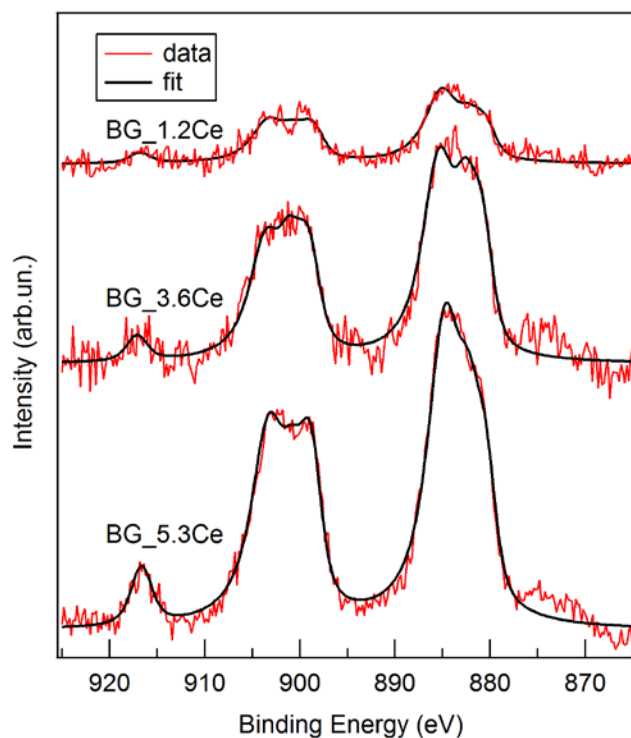


Figure 4. Phosphorous environment in a) BG glass and b) BG_5.3Ce glass; Silicate network polymerization and its environment in c) BG glass and d) BG_5.3Ce glass. Blue and dark yellow tetrahedra are P and Si, respectively. Red, light blue, yellow and green spheres are O, Na, Ca and Ce, respectively.

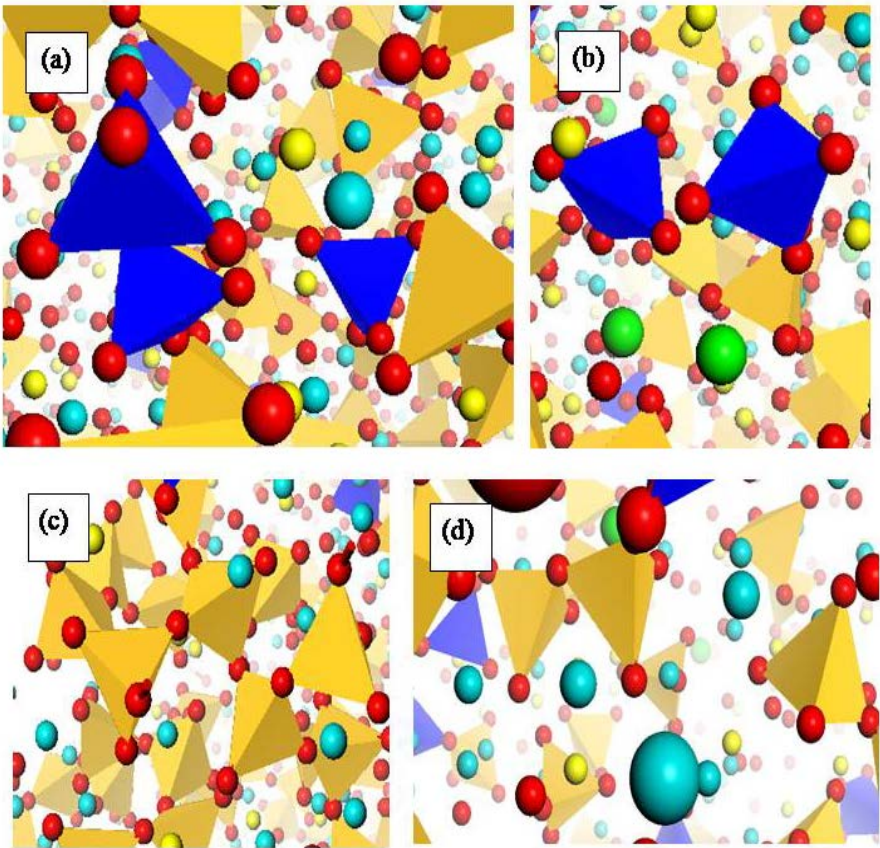


Figure 5. Degradation of (a) H_2O_2 0.1 M and (b) H_2O_2 1 M after soaking of the glasses doped with CeO_2 , BG is reported as control. The lines serve only to guide the eyes.

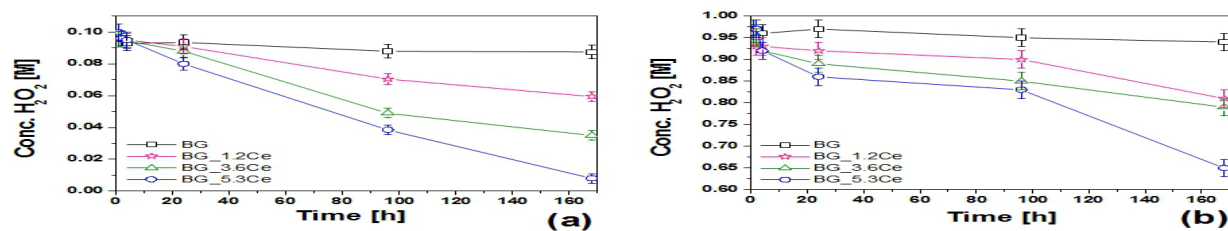


Figure 6. UV-Vis spectra of samples before (AQ) and after soaking in 0.1 M (left) and 1 M (right) H_2O_2 solution at different times.

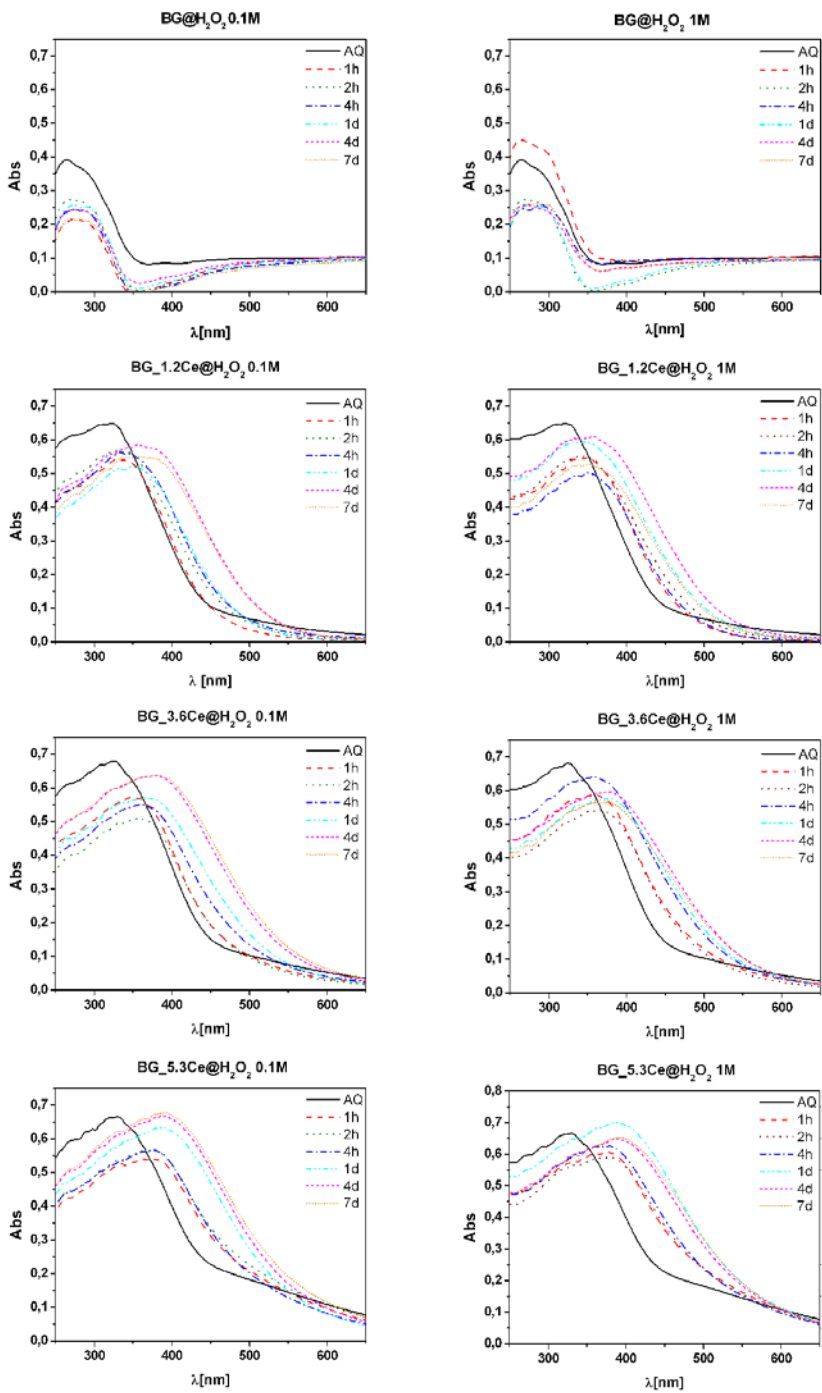


Figure 7. Ce 3d XPS spectra for BG_5.3Ce (red lines) and fitting curves (black lines) after different selected soaking times in 0.1 M (a) and 1 M (b) H_2O_2 solution. The spectra have been normalized in intensity to compare their shape. (c) $\text{Ce}^{3+}/\text{Ce}^{4+}$ ratios obtained from the fitting of Ce 3d XPS spectra as a function of soaking time in the 0.1 M (red dots) and 1 M (blue triangles) H_2O_2 solution; the lines serve only to guide the eyes.

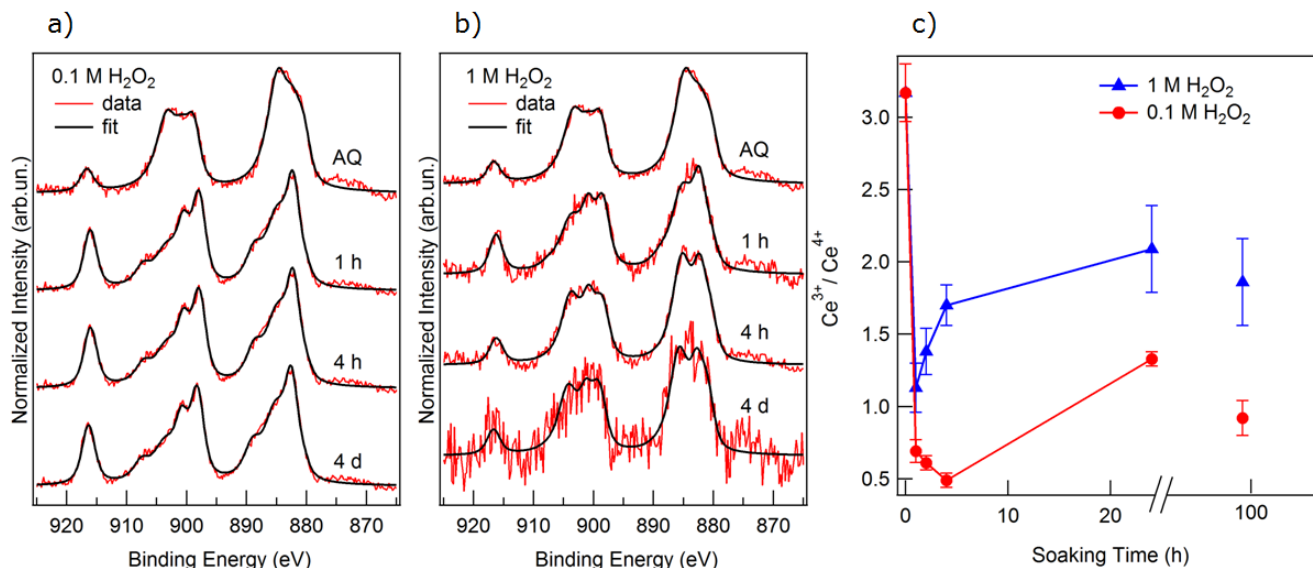


Table of Content



We report the first evidence of catalase mimetic activity of bioactive glasses doped with CeO₂.